Validation of a Rapid Attribution of the May/June 2016 Flood-Inducing Precipitation in France to Climate Change

SJOUKJE PHILIP, SARAH F. KEW, GEERT JAN VAN OLDENBORGH, AND EMMA AALBERS

Royal Netherlands Meteorological Institute (KNMI), De Bilt, Netherlands

ROBERT VAUTARD

LSCE/IPSL Laboratoire CEA/CNRS/UVSQ, Gif-sur-Yvette, France

FRIEDERIKE OTTO AND KARSTEN HAUSTEIN

Environmental Change Institute, University of Oxford, Oxford, United Kingdom

FLORENCE HABETS

METIS/IPSL Laboratoire CNRS/Pierre and Marie Curie University, Paris, France

ROOP SINGH

Red Cross Red Crescent Climate Centre, The Hague, Netherlands

ABSTRACT: The extreme precipitation that resulted in historic flooding in central-northern France began 26 May 2016 and was linked to a large cutoff low. The floods caused some casualties and over a billion euros in damage. To objectively answer the question of whether anthropogenic climate change played a role, a near-real-time "rapid" attribution analysis was performed, using well-established event attribution methods, best available observational data, and as many climate simulations as possible within that time frame. This study confirms the results of the rapid attribution study. We estimate how anthropogenic climate change has affected the likelihood of exceedance of the observed amount of 3-day precipitation in April–June for the Seine and Loire basins. We find that the observed precipitation in the Seine basin was very rare, with a return period of hundreds of years. It was less rare on the Loire—roughly 1 in 20 years. We evaluated five climate model ensembles for 3-day basin-averaged precipitation extremes in April–June. The four ensembles that simulated the statistics agree well. Combining the results reduces the uncertainty and indicates that the probability of such rainfall has increased over the last century by about a factor of 2.2 (>1.4) on the Seine and 1.9 (>1.5) on the Loire due to anthropogenic emissions. These numbers are virtually the same as those in the near-real-time attribution study by van Oldenborgh et al. Together with the evaluation of the attribution of Storm Desmond by Otto et al., this shows that, for these types of events, near-real-time attribution studies are now possible.

KEYWORDS: Climate change; Climate models

---

1. Introduction

From 26 May to 4 June 2016, a low pressure system stayed almost stationary over France and Germany. Due to their differing locations relative to the weather system's center, France and Germany underwent heavy rainfall with different characteristics: moderate but continuous rain, partially large scale, partially convective, over 3 consecutive days in central and northeast France, while severe thunderstorms hit southern Germany.

An analysis of the flooding events in France and Germany was submitted to *Hydrology and Earth System Sciences Discussions* soon after the event but was rejected, partially because the analysis was considered to have been conducted too quickly for peer-review standards and it was written up too hastily. The original manuscript can still be found as a discussion paper (including reviews and replies; van Oldenborgh et al. 2016). The current paper focuses on the French event, reproduces all relevant background information, and compares the results of the current "slow" attribution study, including data that were not yet available in the real-time study, with the real-time results where relevant. This paper can be read independently of the discussion paper.

In France, the sustained precipitation in 2016 came on top of an already wet spring season and affected small river basins. As a consequence, flooding occurred first on smaller rivers like the Yvette and Loing, and later runoff fueled high water levels in the Loire and especially the Seine. The highest 3-day rainfall occurred over 29–31 May (see Fig. 1). Over these three days, moisture contributing to this rainfall converged from multiple sources and moved into the region mainly from

Publisher's Note: This article was revised on 22 December 2021 to correct multiple mistakes with the authors' affiliations when originally published. The first and second listed affiliations above share the first position.

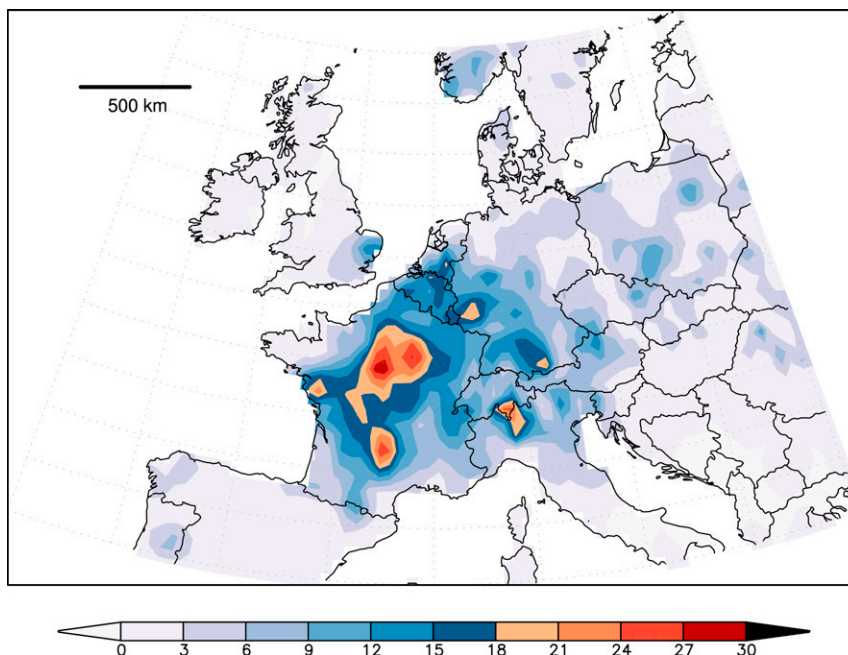*Corresponding author:* Sjoukje Philip, philip@knmi.nl

FIG. 1. Precipitation averaged in western Europe (40°–60°N, 15°W–25°E) over 29–31 May 2016 (mm day^{-1}). Source: NOAA/NCEP/CPC.

the east, circulating around the low pressure system. Potential source regions include the Mediterranean, Baltic, subtropical Atlantic, eastern Atlantic, and moisture recycling over continental Europe.

The maximum amount of rain fell on the center of the Loire basin around the cities of Orléans and Tours (150 mm in 3 days), leading to the flooding of highways on 31 May with numerous drivers being stranded. The famous Renaissance Chambord castle was flooded on 1 June. The floods mostly affected small tributaries with reduced warning systems.

The Loing River, a tributary of the Seine basin, reacted promptly to the heavy rainfall and several cities were flooded on 1 June, with more than 4000 people evacuated at Nemours. It is the most severe flooding event ever reported on the Loing basin. Although only representing a surface area less than 9% of the Seine basin, the Loing River contributed to around 25% of the flood peak of the Seine. The Yvette River, a small tributary in a heavily urbanized area southwest of Paris, flooded several cities on the morning of 2 June, resulting in more than 2000 evacuees in Longjumeau. The Seine crested in Paris on 3 June at a height above 6.1 m at the reference gauge for the Seine at Paris, Paris Austerlitz. This was not a record on the Seine River. The water level was lower than during the major flood of 1910 and was also lower than the floods in 1924, 1945, 1955, 1959, and 1982. The Seine flood itself is estimated to have a return period of about 20 years (Brunelle et al. 2016). There was considerable damage upstream of Paris, with four fatalities (Gallet 2016), thousands of evacuees, thousands without power, and an economic cost estimated above 1 billion euros (Mulholland 2016; Perrin et al. 2017). Estimates indicate that 828 100 inhabitants were exposed to flooding in the Île-de-France, mainly because buildings were constructed before the introduction of regulations that prohibit building in floodplains (Faytre 2011).

However, damages in Paris were less severe. Essential networks that are typically vulnerable to flooding due to their underground location (phone, railway, and sewage) were largely unaffected in Paris, although the Metro line that ran directly along the Seine was forced to close and many people were left without electricity. A timely training of crisis managers conducted in Paris in March 2016, Operation EU Sequana, simulated a major flood in the Île-de-France over 11 days and ensured authorities were prepared (www.prefecturedepolice. interieur.gouv.fr/Sequana/EU-Sequana-2016).

A multireservoir system exists to reduce floods and sustain low flows in the Seine basin. The four reservoirs in the system are operated independently and follow filling curves that determine the target amount of water retained in the reservoir each day of the year. During the high-flow seasons of November–June water is stored in order to maintain the desired flows during the upcoming dry season, a necessary function to regulate water levels for shipping and drinking water for approximately 20 million people, among other socioeconomic benefits (Ficchì et al. 2016; Dorchies et al. 2014). During this flooding event, all of the reservoirs were near 90% full in anticipation of typically dry conditions in the summer months. This flood came as a surprise as large floods in late spring are rare: virtually all Seine floods occur in winter. In the historical record only July 1659 and June 1856 recorded floods outside of the extended winter (December–March), and the observed river flow on 2 June 2016 in Paris was 46% above the previous records in June available since 1886, which was 933 m^3 s^{-1} in 1926. The defenses currently in

place provide effective protection against frequent small floods and significantly lower the risks of larger floods and the associated damage. However, they are vulnerable to spring flooding when reservoirs are typically almost full in anticipation of drier conditions, as well as to successive flooding events that the dams may lack capacity to moderate (Roche 2004). In addition, while all four reservoirs are located in the upstream areas of the Seine basin, some of the smaller tributaries that encountered the worst flooding during this event are located outside of the reservoir catchment areas. Despite this, the reservoirs are estimated to have reduced the flood peak in Paris by about 0.23 m (-40 m^3 s^{-1}; Seine Grands Lacs 2016).

In this study we perform an attribution analysis of the heavy rainfall event preceding the floods in the Seine and Loire basins (Fig. 2). We consider the basin-averaged precipitation in the 3-day period 29–31 May as the main cause of the floods. Three days is the estimated response time of the river, and the accumulated 3-day precipitation was as much as 56% of the total amount of precipitation during the 16 days preceding the Seine flood peak.

Although heavy rainfall as a variable captures a relevant aspect of the flooding events that occurred, several other contributing factors are not considered here. These include catchment characteristics (e.g., topography, land use, and runoff characteristics), elevated saturation levels at the time of this extreme rainfall event due to a wet spring and the locations, holding capacity, and impacts of the upstream reservoirs filling. A full attribution of the floods themselves, rather than just the rainfall event, would therefore need to take all of these factors into account. The aim of this study is to evaluate the near-real-time attribution study, and not to do a new attribution study of the flood itself.

The attribution of trends in heavy precipitation to human influence has been a focus in recent years (e.g., Pall et al. 2011; Schaller et al. 2016). These pioneer studies showed the potential of providing statements about the role of human activities on weather extremes. However, demand on such information is often in real time, when, for a couple of days, damages and losses raise the attention of the public and media and help policy-makers to trigger new adaptation policies. A challenge is therefore to provide scientifically sound and reliable information in near–real time (about a week) about human influence on extreme events. There is still some debate within the scientific community whether the advantage of a quick analysis that may contain slight "errors" outweighs the benefit of an in-depth analysis that waits for all observational data. We argue that a quick analysis is highly useful and here present a validation study of such a quick analysis. This serves to illustrate that the magnitude difference in results from using updated data is rather small. The first revisited rapid attribution study for the purpose of validation was for the winter storm Desmond by van Oldenborgh et al. (2015), which was considered too hastily written to be acceptable as a scientific paper. However, the results were recently confirmed in Otto et al. (2018).

Considering events similar to the rain studied here, Schaller et al. (2014) found no trend in 3-day rainfall averaged over
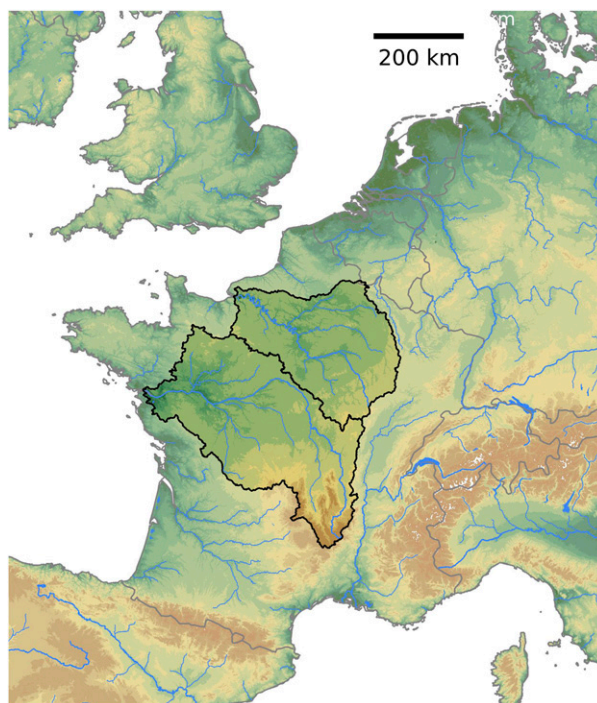

FIG. 2. Maps of the Seine (northern basin) and Loire (southern basin) basins on top of elevation data (http://hydrosheds.cr.usgs. gov; Lehner et al. 2008), including river data.

the upper Elbe and Danube basins in the same late spring/early summer season, whereas Vautard et al. (2015) and Ribes et al. (2018) showed a significant increase of about 5% decade^{-1} in extreme convective autumn rainfalls in a Mediterranean mountain range in southern France over the past 60 years and in surrounding areas.

On a coarser scale, van den Besselaar et al. (2013) studied trends in 1-in-20-year events over 1951–2010, where they divide Europe in a northern and a southern half at 48°N. They found that these events become more common in northern Europe in spring but show no significant change in southern Europe, both for 1- and 5-day periods.

The studies mentioned above show that findings depend on the region, season, and time duration of the event under study. Besides, different datasets or models may lead to different conclusions, which increases the need of multimodel studies.

In this article, we report the results of an attribution of the French 3-day event. This study was originally carried out through collaboration of several organizations, including the team of the World Weather Attribution initiative (https://www.worldweatherattribution.org/) in a time period of less than 10 days. The original study also included an analysis of the 1-day area-maximum precipitation in Germany (van Oldenborgh et al. 2016), showing that an attribution of that event was not possible with the data available at the time. In this evaluation study we only show the results for the two French basins, and we used

additional observational datasets to study the influence of data availability. The trends in the 3-day mean basin-averaged precipitation in France are investigated using a variety of methods, using three observational or reanalysis datasets and five different ensembles of climate models (see Table 1). We computed the trends in observations since 1950, the trends in sea surface temperature (SST)-forced global climate model simulations since 1960, trends in regional climate model simulations since 1950, and comparisons with a counterfactual climate without anthropogenic emissions in a large ensemble of SST-forced regional model simulations. The methodology is described in section 2. The analysis of observations and the five model ensembles are described in sections 3 and 4. Furthermore, in section 5 we briefly analyze the potential large-scale dynamic contribution of anomalous SSTs to the rainfall event. This is followed by a synthesis, discussion, and conclusions in section 6.

2. Methods

The attribution method consists of four steps, which are repeated for the two regions. First, the models are validated for the class of events under consideration. Next, the return period of the observed 2016 event is calculated. The third step is the trend detection. Finally, attribution of the detected trend is done. These steps are described below.

First, we evaluate whether the observational analyses and models represent the statistics of high spring precipitation well enough to be able to use them. We do this mainly by fitting the 3-daily extremes in April–June to a generalized extreme value (GEV) distribution (Coles 2001), which is assumed appropriate for these block maxima. The event itself is excluded from the fits. To account for possible changes, we scale the distribution with a measure of climate change, for which we take the 4-yr smoothed global mean temperature anomaly T'. The smoothing is introduced to remove the fluctuations in the global mean temperature due to ENSO, which are unforced. This measure was already used in van Oldenborgh (2007). [Taking other measures, such as the CO_2 concentration or radiative forcing estimates, gives almost the same results as these are highly correlated: for annual means, the Pearson correlation coefficient is $r(T', CO_2) = 0.93$.]

The scaling is taken to be an exponential function of the smoothed global mean temperature. This exponential dependence can clearly be seen in the scaling of daily precipitation extremes with local daily temperature in regions with enough moisture availability (Allen and Ingram 2002; Lenderink and van Meijgaard 2008). It is also expected on theoretical grounds through the first-order dependence of the maximum moisture content on temperature in the Clausius–Clapeyron (CC) relations of about 7% K^{-1}, which gives rise to an exponential form. Note that we fit the strength of the connection, which is often different from CC scaling. As it is not clear what the relevant local temperature is, but local temperature usually scales linearly with the global mean temperature, we chose the latter.

Specifically, we take

$$F(p) = \exp\left[-\left(1 + \xi \frac{p - \mu}{\sigma}\right)^{1/\xi}\right],$$
$$\mu = \mu_0 \exp(\alpha T'/\mu_0),$$
$$\sigma = \sigma_0 \exp(\alpha T'/\mu_0), \tag{1}$$

with p the precipitation. We refer to μ as the location parameter, σ as the scale parameter, and ξ as the shape parameter. We assume that the ratio σ/μ, also called the dispersion parameter, is constant, reducing the number of fit parameters. This is a standard method in hydrodynamics, where it is called the index flood assumption (e.g., Hanel et al. 2009). We check that it also holds here in models with enough data that this assumption does not need to be made.

The fit is performed using a maximum likelihood method varying α, μ_0, σ_0, and ξ. Uncertainties are estimated with a 1000-member nonparametric bootstrap. In the bootstrap we take all years to be independent, which is supported by the lack of serial autocorrelations in the data. When fitting to sets of stations (section 3) or ensembles of model simulations (sections 4a–4e), we have to take correlations between neighboring stations or similar ensemble members into account. This is done with a moving block technique analogous to the standard overlapping moving blocks employed when a time series has significant serial autocorrelations (e.g., Efron and Tibshirani 1998). In that case the block length is set by the time at which the autocorrelation drops to $1/e$. Here, we take bootstrap samples of blocks of stations with correlation $r > 1/e$. In practice this means that after selecting a random year and station, all stations that have a correlation as high as this are also entered into the bootstrap sample, just like a block of years would have been selected in the case of serial autocorrelations. As a check, we redid the analysis of Vautard et al. (2015) with this technique and verified that we obtained the same result. The same spatial moving block technique was also used in Eden et al. (2016) and van der Wiel et al. (2017).

The shape parameter ξ is considered to be unphysical if larger than 0.4 (a very heavy tail). We therefore implement a penalty term on ξ with a width of 0.2. It can be seen from the fits in the analysis that $|\xi| < 0.1$ for the 3-day mean basin-averaged precipitation. For daily maximum precipitation there are arguments that $\xi \approx 0.12$ (Wilson and Toumi 2005; van den Brink and Können 2011). All these values are substantially less than the cutoff and are therefore virtually unaffected by the penalty term. Conversely, time series often have high outliers (cf. van den Brink and Können 2008). In the bootstrap procedure, replicating these outliers multiple times gives fits with unphysically high values of the shape parameter. The penalty function does not affect the best fit but keeps these unphysical fits from the sample that is used to estimate the uncertainties.

After fitting Eq. (1) to the data, we verify that the underlying assumptions are not invalid. Specifically, the return period plots show whether the distribution can be described by a GEV by overlaying the data points and fit for the present and a past climate. Deviations, such as those caused by double

TABLE 1. Observational, reanalysis, and model datasets used in this study. Datasets are explained in more detail in the relevant sections.

Data		Description	SST	GHG and aerosol forcing	Resolution	Period
Observations						
E-OBS (12.0) 14.0		Gridded station data	—	—	0.25°	1950–now
CPC		Gridded station data	—	—	0.50°	1979–now
ERA-Interim		Reanalysis field	—	—	80 km	1979–now
Model ensembles						
HadGEM3-A	Historical	15-member GCM, atmosphere only	Observed	Historical until 2005, RCP4.5 from 2005 to 2013	60 km	1960–2013
	Natural	15-member GCM, atmosphere only	Natural	Natural	60 km	1960–2013
EC-Earth 2.3		16-member GCM	Coupled	Historical until 2005, RCP8.5 from 2005 to 2016	150 km	1860–2016
weather@home	Historical	1100- (2200) member 2014 (2015) RCM HadRM3P, downscaled from GCM HadAM3P, atmosphere only	Observed	Historical	50 km	2014–15
	HistNat	3000- (4700) member 2014 (2015) RCM HadRM3P, downscaled from GCM HadAM3P, atmosphere only	Natural	Natural	50 km	2014–15
	HistClim	200 members per year RCMHadRM3P, downscaled from GCM HadAM3P, atmosphere only	Observed	Historical	50 km	1986–2014
RACMO-EC-Earth		16-member RCM, downscaled from GCM EC-Earth2.3	Coupled	Historical until 2005, RCP 8.5 from 2006 to 2015	0.11°	1950–2015
EURO-CORDEX		Multimodel (9) RCM, downscaled from different GCMs	Coupled	Historical until 2005, RCP 8.5 afterward	0.11°	1950 to 1971–2015

populations when the most extreme events are caused by a different mechanism with different GEV properties, are clearly visible on this plot. It is similar to the usual Q–Q plot but with axes emphasizing the high extremes. The second assumption, that the PDF scales with the smoothed global mean temperature, is checked in the weather@home model (section 4c). The high number of data points means that the extremes in that model can be studied without these assumptions.

The three parameters of the distribution, μ, σ, and ξ, are evaluated for the year 2016 (using the 3-yr average of 2014–16 as estimate of the smoothed temperature of 2016) and the values for the observational estimates (analyses and reanalysis) compared. Models are evaluated by checking whether these parameters are similar to the distribution fitted to the longest observational analysis. We require that for the models, both the ratio of σ/μ and ξ should be comparable to those estimated from observations within the 95% confidence interval (CI). If this is the case, we apply a multiplicative bias correction, if necessary, to account for differences in the model mean compared to observations.

After the model evaluations, the return period of the observed 2016 event is calculated. We determine the return periods from the GEV distributions for the year 2016. As explained above, for models, if necessary, this is calculated after applying a multiplicative bias correction when the model fitted range of μ does not overlap with the fit from observations.

The next step is trend detection. For the observed record and reliable models for which simulations of the historical record are available, we fit Eq. (1) to the maxima of all available years. Inserting the T' for the years 1960 (or the first year with data if later) and 2016 in Eq. (1) gives the probability for the event in these years, p_0 and p_1. These are expressed as return periods $\tau_i = 1/p_i$. The ratio of these is commonly referred to as the risk ratio, RR = $p_1/p_0 = \tau_0/\tau_1$. If this ratio is significantly different from one, that is, the bootstrapped two-sided 95% confidence interval excludes one, a trend is detected. The p value of the lower bound being positive is estimated as $p = (N_{\leq 0} + 1)/(N + 1)$ with $N = 1000$ the number of bootstrap members and $N_{\leq 0}$ the number with zero or negative trend ($\alpha \leq 0$ or equivalently RR ≤ 1). If we have a priori knowledge that the trend should be positive, we can interpret this as a test that the trend is positive at $p < 0.025$; if this knowledge is lacking, this is a test that the trend is not zero at $p < 0.05$. The trend indicates how much more likely the event is now than in 1960, but does not attribute this difference.

To attribute the change, we use models for which we also have experiments simulating a counterfactual world without anthropogenic emissions of greenhouse gases and aerosols. These allow us to compute how much more likely or unlikely the event has become due to these emissions. Often we can neglect the effect of natural forcings on these extremes. In that case the modeled change from preindustrial conditions to now (about 1°C warming) can also be used for attribution. Given the assumption of exponential dependence on temperature in Eq. (1), we transform the risk ratios from 1960–2016 to 1880–2016, which is close to preindustrial–2016 (Hawkins

et al. 2017), by assuming that the logarithm of the risk ratio depends linearly on the global mean temperature.

Because single models usually do not give a reliable description of trends in the climate system due to model biases (Annan and Hargreaves 2010; Yokohata et al. 2012; van Oldenborgh et al. 2013), we use as many (preferably multimember or long runs and high resolution) model ensembles as readily available. In seasonal forecasting and attribution studies such an ensemble represents the uncertainty better than a single model (Hagedorn et al. 2005; Hauser et al. 2017). A last step is therefore to synthesize the results into a single attribution statement. The differences among the RRs of these ensembles and the observations are due to natural variability and to model spread. The relative contribution of each of these factors can be determined from a χ^2 statistic. We compute χ^2/dof, with the number of degrees of freedom (dof) one less than the number of fits. If this is roughly equal to one, the variability is compatible with only the natural variability that determines the uncertainty on each separate model estimate of the RR. If it is much larger than one, the differences between the models contribute significantly.

If the natural variability dominates, which is often the case for precipitation, the final result can be obtained by a simple average RR. We choose to use a weighted average, with for each RR (models and observations) the weights are the inverse uncertainty squared, as the uncertainty due to natural variability is smaller in models with much data. The uncertainties are approximated by symmetric errors on log(RR) and added in quadrature $\varepsilon^2 = \sqrt{\varepsilon_1^2 + \varepsilon_2^2 + \ldots + \varepsilon_2^N}/N$. If there is a significant contribution of χ^2 due to model spread, this has to be propagated to the final result, and the final uncertainty is larger than the spread due to natural variability would indicate. In this case we choose to give all models equal weight. The method described here was also used in Eden et al. (2016).

3. Observational analysis

New in this analysis compared to the rapid analysis is the use of an updated dataset—E-OBS 14.0 instead of E-OBS 12.0. This update includes additional French station data that were not available in real time. The analyses in the rejected manuscript were based on a relatively sparse subset of stations. Updated numbers are given to compare to the rapid analysis.

We compare the 0.25°E-OBS 14.0 analysis 1950–2016 (Haylock et al. 2008) and 0.5° CPC analysis 1979–2016 (www.cpc.ncep.noaa.gov/products/Global_Monsoons/gl_obs.shtml). The decorrelation scales of 3-day mean precipitation in this season are more than 100 km (derived from the public dense Dutch station network; we cannot determine how much larger because of the limited size of that country). This is large enough that station sparsity is not a problem. We double-checked this by comparing the basin averages with the ERA-Interim reanalysis, which is completely independent, and found good agreement. Satellite-derived products do not perform well in this region and season, exemplified by a correlation of only $r = 0.7$ for 3-day Seine basin-averaged
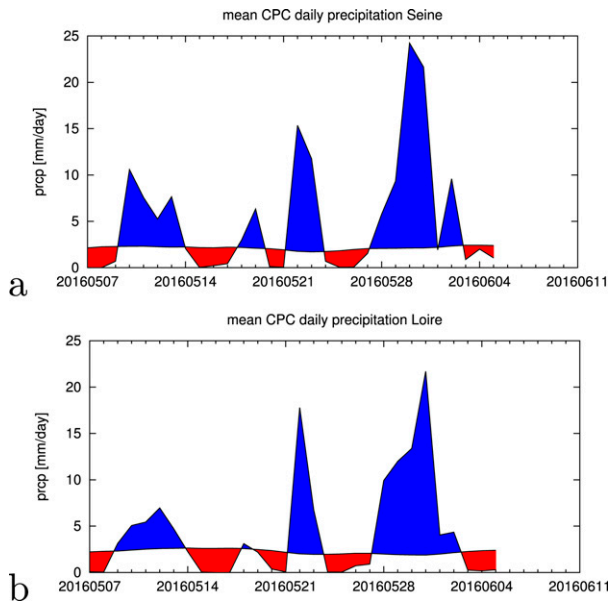
FIG. 3. CPC analyzed sums of precipitation averaged over the (a) Seine and (b) Loire basins. The smooth line denotes the 1981–2010 climatology.

precipitation with E-OBS 14.0 over earlier years. Radar data cannot be used for attribution due to the short time series and large biases until it is calibrated against station data.

The CPC analysis, which is updated daily, shows the highest sums over 29–31 May 2016: in the original manuscript, the 3-day mean averaged over the Seine basin was 18.4 mm day^{-1} [corresponding to a sum of 55.2 mm (3 days)$^{-1}$] and 15.7 mm day^{-1} [sum of 47.1 mm (3 days)$^{-1}$] for the Loire basin (see Fig. 3). These values were taken to represent the observed event, as the E-OBS data for 29–31 May 2016 were not yet available at the time the rapid manuscript was submitted. In this new analysis, the E-OBS 14.0 estimates are 19.2 mm day^{-1} for the Seine and 16.1 mm day^{-1} for the Loire, which are within 5% of the initial estimates. The Safran reanalysis (Quintana-Seguí et al. 2008), which also became available much later, gives 20.3 mm day^{-1} for the Seine and 19.0 mm day^{-1} for the Loire, 10% and 21% more than the initial

estimates. These differences do not affect the conclusions. Comparisons are noted in the text.

For the 3-day mean and basin-averaged precipitation the distributions of the CPC and E-OBS 14.0 analyses are remarkably similar, even though they cover different time periods (see Tables 2, 3). The shorter ERA-Interim reanalysis also resembles these well, albeit with a slightly smaller-scale parameter. We performed a GEV fit using Eq. (1), which includes a trend analysis by fitting the trend parameter α. It suggests that the return period for the Seine basin is larger than the length of the longest series, which is E-OBS 14.0: $\tau_1 > 250$ years for such an event in April–June. (Note that a fit to an extreme value distribution can only determine a return period smaller than about $2N$ years from a series of length N years with accuracy.) The time series from 1950, Fig. 4a, shows how unusual this amount is for late spring/early summer. The best fit for the trend parameter α is positive. However, the uncertainties are large and easily encompass $\alpha = 0$ or equivalently RR = 1.

For the Loire basin the event was less exceptional in April–June, with a return time of about 50 years (11–4000 years) in a GEV fit. The risk ratio again encompasses one, RR = 40(0.7 → ∞).

The model analyses in the next sections show that for higher statistics the shape parameter ξ is very close to zero. We can reduce the uncertainties in the estimate of the return period by setting $\xi = 0$, that is, assuming a Gumbel distribution (Fig. 5). In the original manuscript this gave a best estimate for the return period of 180 years for the Seine basin for the E-OBS 12.0 historical series in the current climate (as used in the near-real-time attribution), with still a wide 95% uncertainty range of 50–3000 years. Using E-OBS 14.0 for both the historical time series and the value for 2016, we find a somewhat higher value of 260 years (60–6000 years); however, this is well within the uncertainties of the earlier estimate. This fit gives a RR of 2.1 (0.3–14).

The 3-day rainfall in the Loire basin was less exceptional: using the data available at the time of the near-real-time attribution, the 2016 precipitation value is not far above the precipitation values in the past years (Figs. 4b,d), with a return period of the order of 100 years in April–June (2.5% lower bound 15 years). The observations also showed a positive trend that was not significantly different from zero. A Gumbel

TABLE 2. Summary of the fits of the data for the Seine: location parameter μ, the scale parameter σ, and the shape parameter ξ of the GEV fit for 2016. Values between parentheses denote the 95% CI. The models that did not pass the validation test are in italic.

Seine dataset	μ (mm day^{-1})	σ (mm day^{-1})	ξ
CPC	7.1 (6.7 to 7.6)	1.8 (0.9 to 1.5)	−0.35 (−0.14 to 0.11)
E-OBS 14.0	7.8 (7.2 to 8.2)	2.0 (1.4 to 2.3)	−0.15 (−0.21 to 0.10)
ERA-interim	7.6 (6.9 to 8.2)	1.7 (1.2 to 2.0)	−0.12 (−0.17 to 0.10)
HadGEM3-A	9.2 (9.1 to 9.4)	2.2 (2.1 to 2.4)	−0.004 (−0.049 to 0.047)
HadGEM3-A Nat	8.8 (8.6 to 9.0)	2.4 (2.2 to 2.5)	−0.049 (−0.093 to 0.000)
EC-Earth	*9.0 (8.9 to 9.1)*	*1.7 (1.7 to 1.8)*	*−0.018 (−0.050 to 0.006)*
weather@home	7.6 (7.5 to 7.7)	2.2 (2.1 to 2.3)	−0.03 (−0.04 to −0.015)
RACMO	8.2 (8.1 to 8.4)	1.8 (1.6 to 1.8)	−0.010 (−0.075 to 0.028)
CORDEX	9.0 (8.8 to 9.2)	2.1 (1.8 to 2.3)	−0.05 (−0.11 to 0.03)

TABLE 3. As in Table 2, but for the Loire.

Loire dataset	μ (mm day^{-1})	σ (mm day^{-1})	ξ
CPC	8.9 (8.2 to 9.7)	2.4 (1.6 to 2.8)	−0.14 (−0.46 to 0.04)
E-OBS 14.0	8.7 (8.3 to 9.2)	2.0 (1.4 to 2.4)	−0.13 (−0.22 to 0.09)
ERA-interim	9.0 (8.3 to 9.8)	1.9 (1.2 to 2.3)	−0.05 (−0.30 to 0.22)
HadGEM3-A	9.4 (9.2 to 9.5)	2.1 (2.0 to 2.2)	−0.027 (−0.074 to 0.026)
HadGEM3-A Nat	9.3 (9.1 to 9.5)	2.0 (1.8 to 2.1)	−0.06 (−0.11 to −0.02)
EC-Earth	*14.2 (14.0 to 14.3)*	*2.8 (2.6 to 2.8)*	*−0.04 (−0.07 to −0.01)*
weather@home	7.8 (7.7 to 7.9)	2.2 (2.1 to 2.3)	−0.035 (−0.045 to −0.015)
RACMO	8.3 (8.2 to 8.4)	1.6 (1.5 to 1.7)	−0.04 (−0.09 to 0.00)
CORDEX	9.5 (9.3 to 9.7)	1.8 (1.7 to 2.0)	−0.01 (−0.07 to 0.05)

fit gave a return period of 35 years (10–300 years). Now, using the E-OBS 14.0 estimate that was available half a year later, the best estimate is 20 years (7–170 years), which is compatible with the earlier estimate. The RR is 5.0 (0.7–30).

In the synthesis, we use the numbers obtained with Gumbel fits to E-OBS 14.0 for observations.

4. Model analyses

We use a set of different climate model ensembles in order to study both natural variability within models and uncertainties that arise from using different models and model setups. In this study we investigate five different model ensembles which cover different model setups: an SST-forced global climate model (HadGEM3-A), a coupled global climate model

(EC-Earth 2.3), regional climate models driven by coupled GCMs (the RACMO-EC-EARTH and EURO-CORDEX ensembles), and a very large ensemble of an atmosphere-only regional climate model (HadRM3P utilizing the weather@home framework). Besides the necessity of being publicly available, the models are selected to have a large number of simulated years. The models are described in more detail in the next subsections.

Every model setup is subjected to some validation tests (see also section 2). Based on the outcome of these tests we either analyze the model or reject it. The parameters σ, μ, and ξ used for these validations are shown in Tables 2 and 3.

Each subsection starts with a description of the model setup, followed by validation tests. For the models that are rejected, the analysis results are not shown.
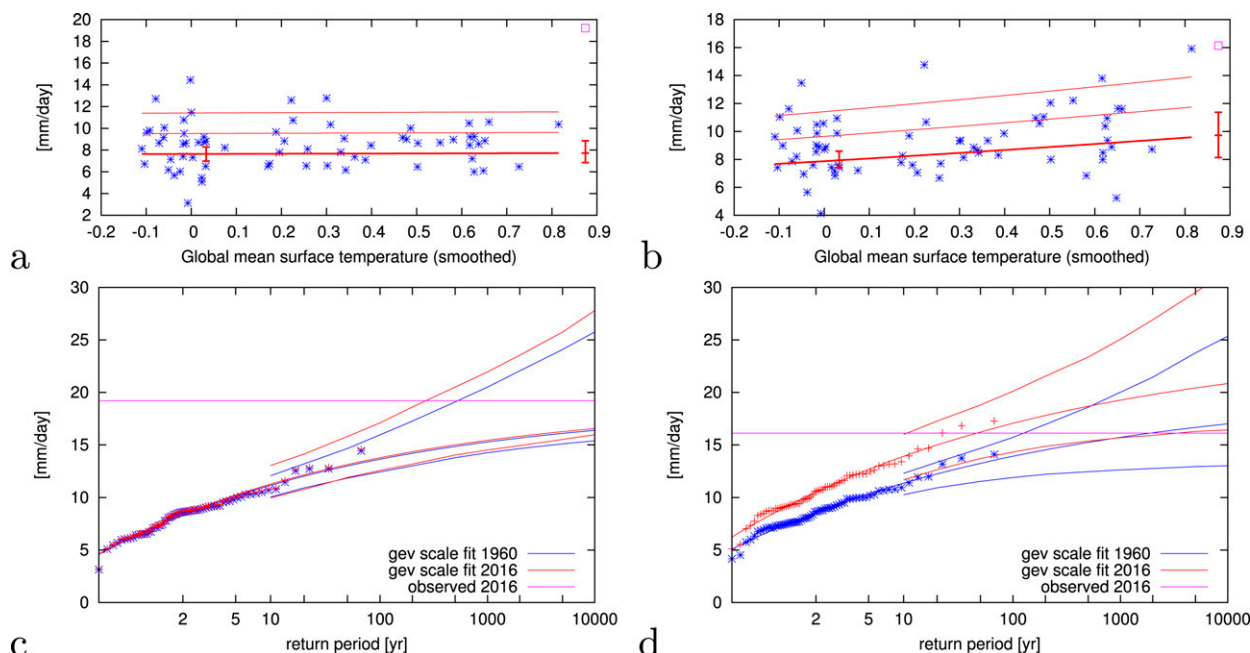

FIG. 4. Fit of the highest observed 3-day mean rainfall in the Seine basin in April–June to a GEV that scales with the smoothed global mean temperature. (a) The location parameter μ (lower line), $\mu + \sigma$, and $\mu + 2\sigma$ (middle and upper lines). The vertical bars indicate the 95% confidence interval on the location parameter μ at the two reference years. The purple square denotes the value of 2016 (not included in the fit). (c) Gumbel plot of the GEV fit in 2016 (red lines) and 1960 (blue lines). The observations are drawn twice, scaled up with the trend to 2016 and scaled down to 1960. (b),(d) As in (a) and (c), but for the Loire. Data from E-OBS 14.0.
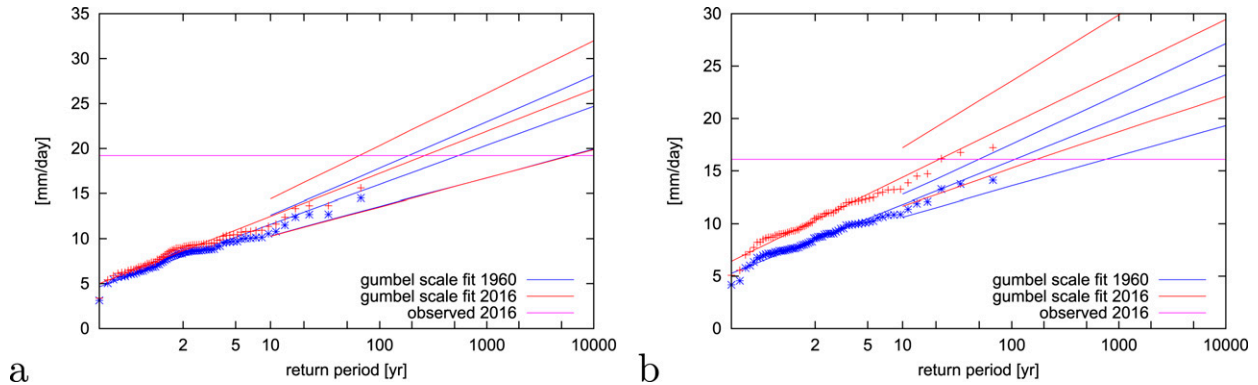
FIG. 5. As Figs. 4c and 4d, but assuming a Gumbel distribution, that is, $\xi = 0$, and the E-OBS 14.0 data.

a. HadGEM3-A ensemble

In the European Climate Extremes Interpretation and Attribution (EUCLEIA) project, the Met Office model HadGEM3-A (Christidis et al. 2013) was run in atmosphere-only mode at high resolution (N216, about 60 km) for the period 1960–2013 with observed forcings and SSTs [historical, based on historical forcings up to 2005 and RCP4.5 afterward from phase 5 of the Coupled Model Intercomparison Project (CMIP5)] and with preindustrial forcings and SSTs from which the effect of climate change has been subtracted (historicalNat). The latter change has been estimated from the CMIP5 ensemble of coupled climate simulations (for details see D. Stone and P. Pall 2016, unpublished manuscript). An empirical relation between SST and sea ice was used to establish the sea ice extent. The simulations were made as an ensemble of 15 realizations for the historical forcings, and another ensemble of 15 realizations were used for the historicalNat forcings. The 15 members were all entered into the fit simultaneously. For this variable the series are sufficiently independent ($r < 1/e$) in spite of the common SST forcing. The data are freely available for noncommercial use.

Comparing the annual maximum of 3-day mean basin-averaged precipitation of the historical runs to the E-OBS 14.0 observations (excluding 2016), the model precipitation is about 15% higher than observed in the Seine basin and about 7% in the Loire basin (Table 2). The scale parameters σ are overestimated by the same factor, and the shape parameters ξ are compatible with the observed distribution so that the model results can just be scaled back with a simple bias correction (see also Vautard et al. 2018).

Over the Seine basins, the model shows a clear increase in 3-day extreme precipitation in April–June (see Fig. 6, Table 2). The return period for an event like the one observed is about 200 years in the current climate, with a 95% uncertainty range from 100 to 500 years. This is a factor 1.9 (1.1–3.4) more frequent than in 1960, which is significantly different from zero at $p < 0.025$ (derived from the nonparametric bootstrap described in section 2). The return period of the observed Loire precipitation is about 40 years in April–June (23–62 years). In this model the probability increased by a factor 1.2 (0.8–2.4), which is not significantly different from no change.

Repeating the analysis for the historicalNat, we find no trend: α is compatible with zero when fitting Eq. (1). This gives risk ratios RR = 0.95 (0.5–2.2) on the Seine and 1.1 (0.5–1.7) on the Loire. This shows that the natural forcings and SST patterns have not had a large influence on the trend over this period. The return period is constant and 370 years (160–1000 years) for the Seine and 73 years (50–200 years) for the Loire. Comparing the historical and historicalNat return periods in the current climate, we conclude that the probability has increased by a factor of 2.0 over the Seine basin owing to anthropogenic emissions (0.7–5.0), which is not significantly different from no change at $p < 0.05$. Over the Loire basin the factor is 1.1 (0.6–3.1), also not significantly different from no change at $p < 0.05$. However, as the best estimates of the RR in the historicalNat runs are very close to one, we argue that the (just not significant) trend is mostly due to anthropogenic emissions.

b. EC-Earth ensemble

EC-Earth 2.3 is a coupled general circulation model (Hazeleger et al. 2010). We used 16 experiments covering 1860–2100 of this EC-Earth model using the CMIP5 protocol (Taylor et al. 2011), historical forcings up to 2005, and RCP 8.5 afterward (the different scenarios are very close up to about 2030; Kirtman et al. 2013). The resolution of the model is T159, which is about 150 km. This relatively coarse resolution means that the Seine and Loire River basins are only six and nine grid boxes, respectively.

The EC-Earth runs for the Seine and Loire strongly overestimate the mean precipitation and underestimate the skewness, and therefore also overestimate the location parameter μ in the GEV fit. As the scale parameter σ is on the low side, the distribution cannot be scaled to compensate for this bias (see Tables 2 and 3 for the parameters).

For this reason, we do not trust the model results for our two specific domains and time scales. We therefore did not use the EC-Earth model for these events.

c. Weather@home

We use the HadRM3P regional model at 50-km resolution over Europe embedded in a one-way nesting in the atmosphere-only global circulation model HadAM3P in the
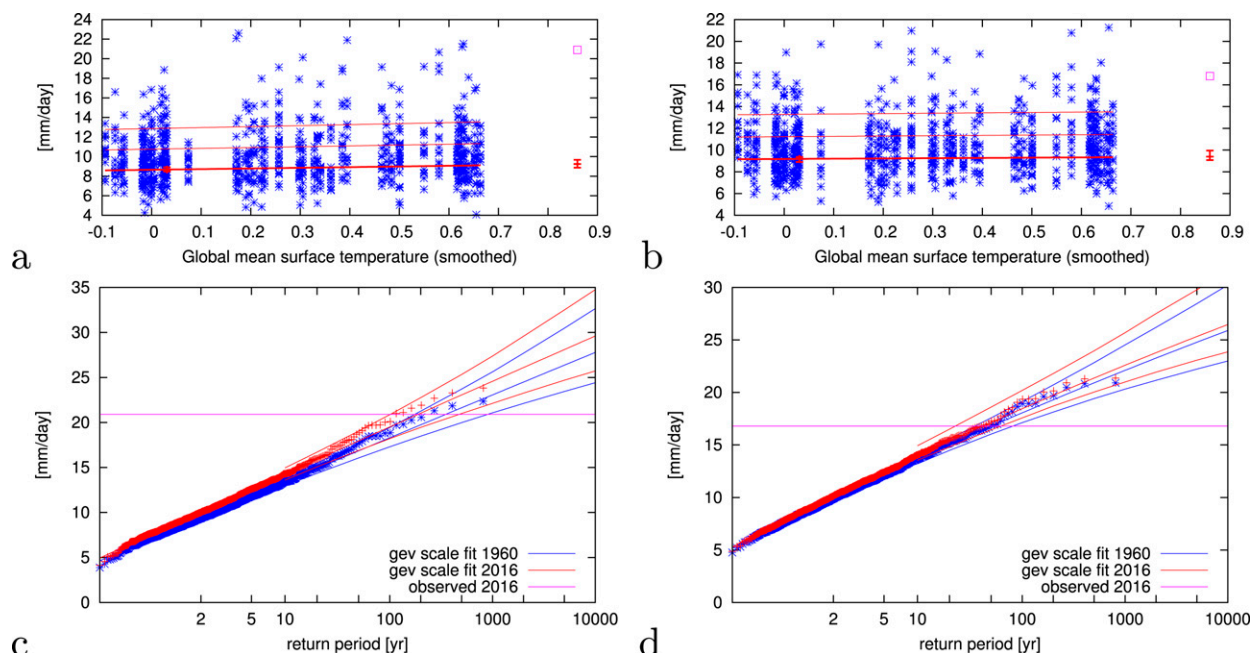
FIG. 6. As in Fig. 4, but for the historical run of the HadGEM3-A N216 model. The 2016 value (horizontal line) has been scaled up to agree with the model bias.

distributed computing framework weather@home (Massey et al. 2015). Three different experiments are used for the analysis: 1) climatology for the period 1986–2014 with observed atmospheric forcings and observed SSTs (historicalClim or CLIM), 2) actual experiment with observed atmospheric forcings and observed SSTs for 2014 and 2015 (historical or ACT), and 3) natural experiment with preindustrial forcings and counterfactual SSTs for 2014 and 2015 (historicalNat or NAT). The actual simulations use current greenhouse gas (GHG) and aerosol concentrations and observed SSTs and sea–ice extent from the Operational Sea Surface Temperature and Sea Ice Analysis (OSTIA) dataset (Donlon et al. 2012). The natural simulations use preindustrial levels of GHGs, multiple anthropogenic warming patterns subtracted from the OSTIA SSTs (as per Schaller et al. 2016), and the maximum observed sea–ice extent in the OSTIA dataset. The climatology serves as a reference dataset for actual simulations and uses OSTIA SSTs.

Different 1-yr-long simulations were produced by varying the initial conditions. Forty starting conditions from previous simulations were used in each scenario, and different initial condition perturbations were applied to the potential temperature to obtain thousands of unique simulations of possible weather. The ensemble size is 200 members per year in the CLIM experiments and 1100 (2200) in ACT and 3000 (4700) in NAT for 2014 (2015). We estimate the maximum 3-day precipitation in simulations of April–June.

The availability of large ensembles has always been the advantage of the weather@home approach to attribution (e.g., Otto et al. 2012; Schaller et al. 2014; Uhe et al. 2016). This makes it possible to estimate changes in return periods

without making assumptions on the shape of the distribution or how it depends on the anthropogenic forcing [the assumptions underlying Eq. (1)]. Comparing the statistics of weather@home simulations to observations, we note that the magnitude of the 3-day running mean maximum in April–June is underestimated by HadRM3P. At the same time the magnitude of 1-day extremes compares well with observations. We believe that this is a model artifact related to insufficient persistence probably in the driving model rather than HadRM3P itself. While the blocking frequency for high pressure systems in HadAM3P compares well with observations (Mitchell et al. 2017), the persistence of summer precipitation has not been assessed yet. Rather than bias correcting the magnitude, we use the best estimate for the observed return period as the event definition to determine the RR in weather@home. This has the same effect as correcting the bias but avoids manipulating the data and potentially destroying the physical consistency of the ensemble (Sippel et al. 2016).

Over the Seine River basin, weather@home shows an increase in 3-day mean extreme precipitation from the experiments for 2014–15 with only natural forcings (NAT) to the experiments with all forcings (ACT, see Fig. 7). Comparing the two experiments at the best estimate of the return period from observations, 370 years, we conclude that the probability of an extreme rainfall event such as observed occurring has increased by a factor of 2.0 over the Seine basin (0.6–5; Fig. 7a, not significantly different from no change). Over the Loire River basin, we find a RR of 1.8 (1.2–2.7; Fig. 7b, significant at $p < 0.05$ based on the 73-yr return period.

Note that the similarity of the curves in Fig. 7 and in the other figures justifies the assumptions made in the other
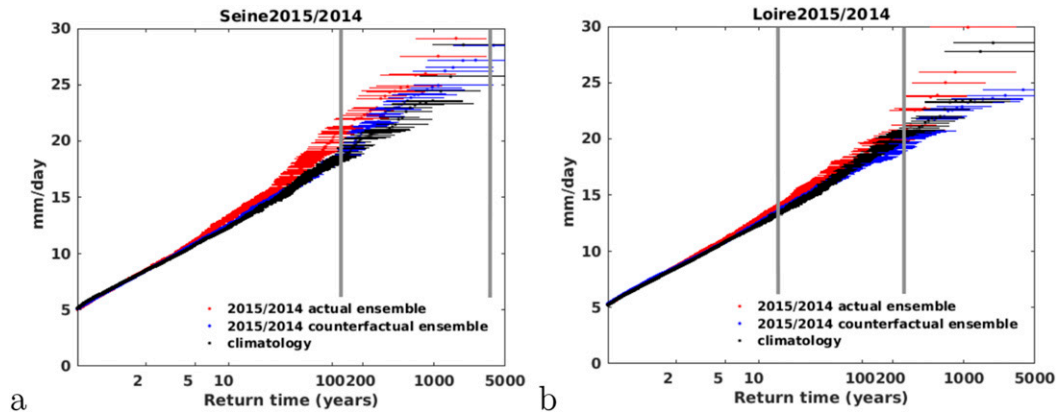
FIG. 7. Return periods for 3-day mean precipitation in April–June 2014 and 2015 from HadRM3P-EU for the (a) Seine and (b) Loire River basins. Red dots are return periods for current conditions (ACT) with the horizontal lines denoting 95% confidence intervals, blue for counterfactual conditions (NAT), and black denotes climatological conditions (CLIM) for the 1986–2014 baseline period. No bias correction has been applied (see text), and the vertical gray lines indicate the range of return times from the observations.

analyses. The first is that the distributions are described well by a GEV (also verified in each plot by the quality of the fit to the data points). The second one, which can only be checked here, is that this GEV scales with global warming. There are no indications that the difference between the red and blue curves in Fig. 7 is different from the other model analyses (Figs. 4, 6, 8) beyond the uncertainties indicated by the 95% error bars.

d. RACMO–EC-Earth ensemble

We use a regional downscaling of the 16 member EC-Earth 2.3 ensemble over western Europe using the RCM KNMI-

RACMO2 (Van Meijgaard et al. 2008; van Meijgaard et al. 2012). RACMO2 is run 16 times at a resolution of 0.11°(12 km) for the period 1950–2100, using initial conditions and boundaries derived from the corresponding EC-Earth members. The RACMO2–EC-Earth ensemble members only differ because of internal variability. Thus, for the period 1950–2015 the ensemble provides 16×66 years of high-resolution data. Although this model cannot yet resolve thunderstorms, it is expected that, owing to the relatively high resolution, it reproduces small-scale extremes better than the ≈150-km EC-Earth
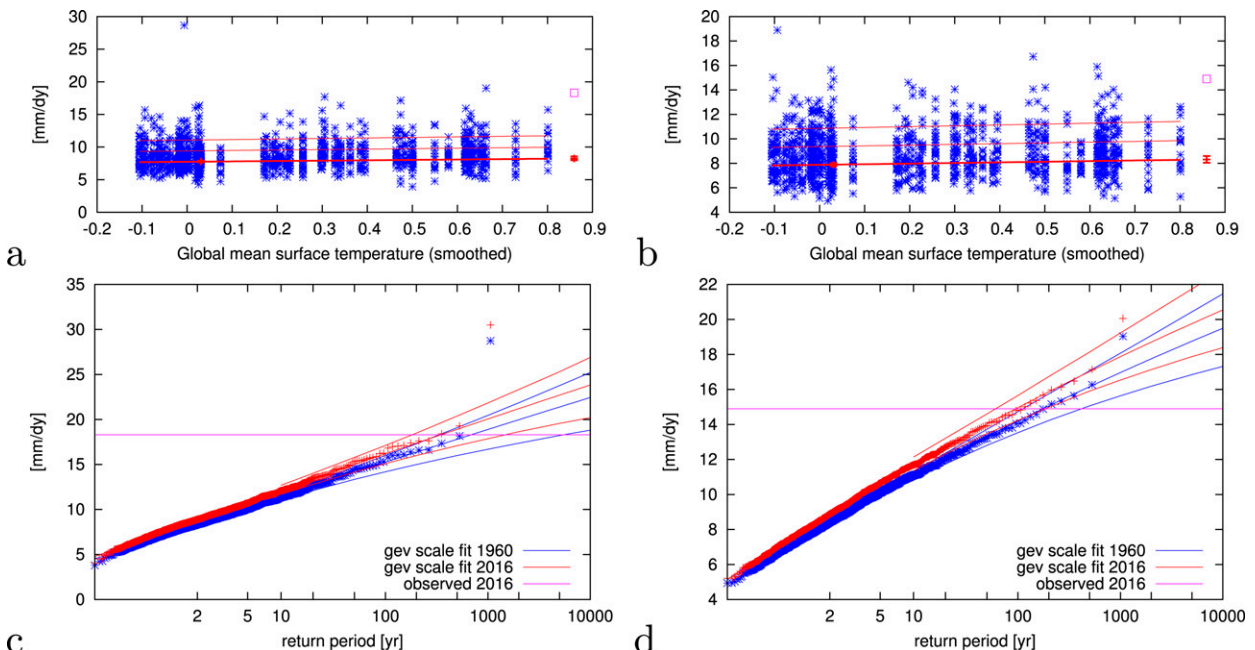

FIG. 8. As in Fig. 4, but for the RACMO data. The observed value (horizontal line) for the Loire has been scaled down by 5% to compensate for the model bias.
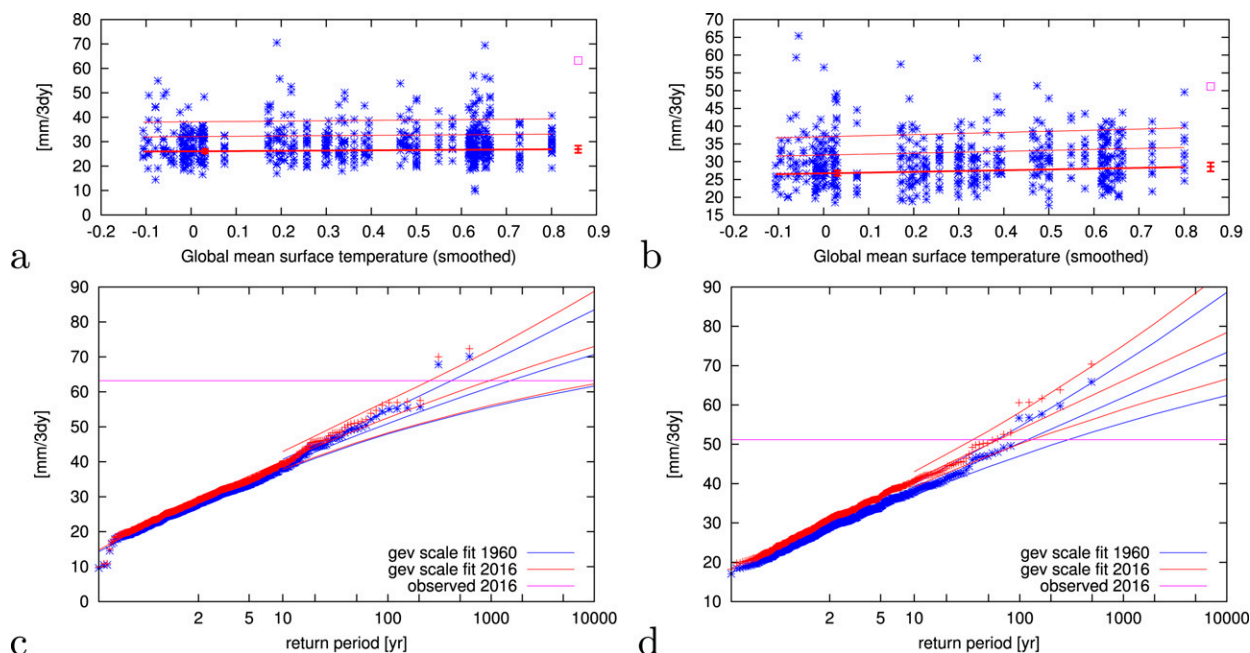
FIG. 9. As in Fig. 4, but for 3-day means in the CORDEX data.

ensemble, the ≈60-km HadGEM3-A ensemble, and the 50-km HadRM3P weather@home ensemble (Prein et al. 2015).

The GEV fit parameters for the Seine are compatible with the fit to the observations (Tables 2, 3) within the 2σ uncertainties, so we accept the model for this analysis and do not apply a bias correction. In the Loire region the model results are just significantly different, about 5% lower than the observed ones in both μ and σ, so we accept the model also for this and apply a small, multiplicative bias correction.

The RACMO ensemble gives a return period in the current climate of 350 years (180–1500 years; see Fig. 8). The probability of an event like the observed one increases with a factor of 2.0 (1.3–4.9), which is different from no change at $p < 0.01$. On the Loire, the return period is about 100 years (60–180 years) and the RR is 1.8 (1.3–3.2), again very significantly different from no change ($p < 0.01$).

e. EURO-CORDEX ensemble

The multimodel EURO-CORDEX ensemble (Jacob et al. 2014) was designed to provide a coordinated set of climate projections at a relatively high resolution (12 km) over Europe and part of the North Atlantic, similar to the RACMO ensemble but multimodel. We used a subset of the EURO-CORDEX climate projections. The simulations all include the historical period starting from dates between 1950 and 1971. We used nine runs using historical forcings up to 2005 and the RCP 8.5 scenario 2006–15. Up to 2030 the RCP scenarios do not diverge noticeably (Kirtman et al. 2013). The runs are CNRM-CM5 r1i1p1/SMHI-RCA4 (1970–2015), EC-EARTH r12i1p1/SMHI-RCA4 (1970–2015), EC-EARTH r1i1p1/KNMI-RACMO22E (1950–2015), EC-EARTH r3i1p1/DMI-HIRHAM5 (1951–2015), IPSL-CM5A-MR r1i1p1/IPSL-

INERIS-WRF331F (1951–2015), IPSL-CM5A-MR r1i1p1/SMHI-RCA4 (1970–2015), HadGEM2-ES r1i1p1/SMHI-RCA4 (1971–2015), MPI-ESM-LR r1i1p1/MPI-CSC-REMO2009 (1950–2015), and MPI-ESM-LR r1i1p1/SMHI-RCA4 (1971–2015). These all have different biases in the annual maximum of 3-day mean precipitation averaged over the river basins. These are corrected to first order by a simple scaling to a common mean, for which the mean of all simulations is taken. Note that the common driving GCMs and RCMs imply that these experiments are not all independent. The same moving block procedure employed for the station data found that there are only 4–5 degrees of freedom in these nine ensemble members. The uncertainties take this into account as detailed in section 2.

The distributions of the annual maximum of April–June 3-day mean basin-average precipitation over the Seine and Loire have shapes that resemble the observed distributions well enough after the multiplicative bias correction. For the Seine we find a return period of about 1000 years (>250 years) with an RR of 1.6 (0.5–4.9; see Fig. 9). Although positive, this is not significantly different from no change. For the Loire basin the return period is around 60 years (36–130 years) with an RR of 1.9 (1.1–3.6), which is significantly different from no change at $p < 0.05$.

5. SST influence on precipitation

Since a smaller ensemble of weather@home HadAM3P global simulations is available for May 2016 [seasonal forecast SSTs from March applied according to the method described in Haustein et al. (2016)], we are able to diagnose the potential large-scale dynamic contribution that current SSTs might

have had on the European floods, such as a lagged effect of the strong 2015/16 El Niño event. Modeled monthly zonal 200-hPa wind anomaly data (w.r.t. 1986–2014) from 200 ACT simulations are used for that purpose. The result can then be contrasted with the change in risk due to thermodynamically driven, warming- related modifications of the background atmosphere. Based on the results with May 2016 SSTs, we found no significant large-scale contribution of anomalous SST patterns to circulation anomalies over Europe. In other words, the zonal wind anomalies at 200 hPa do not indicate that the large-scale flow over Europe was different compared to the climatological mean (1986–2014) in the model.

However, this does not mean that there was no case-specific contribution, as summer circulation anomalies are fairly weak in general and extreme weather is usually driven by other factors, such as mesoscale convection-triggered but rather small cutoff lows. In fact, the weather@home CLIM experiment (black dots in Fig. 7) does suggest a strong role for case-specific dynamic anomalies in the case of the Seine event (less so for the Loire) as intensities for heavier rainfall events are lower in CLIM than even in NAT (for 2014/15). We did not investigate the root cause for that outcome, but note two known effects. First, long-term observations show on average a wetter spring after an El Niño (van Oldenborgh et al. 2000) and higher Seine runoff ($r \approx 0.4$ between April–June runoff at Paris and 2-month-lagged Niño-3.4). The positive SST in the ENSO region during spring 2015 (developing El Niño) could have contributed to the offset between current SST conditions and climatology. Second, North Atlantic SSTs have been connected to the decadal variability in French river runoff (Boé and Habets 2014). These were similar in all three years. Therefore, our main weather@home results based on simulations with 2014/15 SSTs should not give completely different answers for 2016 as far as the RR and the dynamic features are concerned.

The ENSO state in 2016 should increase the likelihood of wet extremes even more than in 2015, so we conclude on the basis of these weather@home results and previous investigations that specific SST patterns, notably El Niño and the Atlantic Ocean, probably increased the risk of flooding in May 2016.

While specific SST patterns in 2015/16 may have influenced the risk of the flooding in May 2016, they cannot explain the existence of a trend in risk. Our results show that climate change is responsible for the trend.

6. Synthesis, discussion, and conclusions

a. Return period

Major floods on the Seine River are rare this time of the year. Although the overall return time of the flood crest at Paris was about 20 years, only two late spring/summer floods have been recorded there in over 500 years before 2016. We computed that a 3-day rainfall event like the one preceding this flood has a return period of a few hundred years in April–June in the Seine basin. The maximum 3-day sum of

TABLE 4. Summary of the return periods of the event in 2016 (except for HadGEM3-A Nat, which is for preindustrial) for the two regions and for all used observations and models. Numbers show the best estimate of the GEV fits (Gumbel for observations) and the 95% CIs (in parentheses).

	Return period
Seine	
E-OBS 14.0	260 (60–6000)
HadGEM3-A	190 (100–500)
HadGEM3-A Nat	370 (160–1000)
RACMO	350 (180–1500)
CORDEX	960 (250–15000)
Loire	
E-OBS 14.0	20 (7–170)
HadGEM3-A	42 (23–62)
HadGEM3-A Nat	73 (50–200)
RACMO	96 (61–180)
CORDEX	62 (36–130)

precipitation averaged over the Loire basin in April–June 2016 has a return period of roughly 20 years. These statements hold for the data that were originally used in the rapid analysis, as well as for the new E-OBS 14.0 data that were used for the current paper.

A summary of the return periods of the 3-day rainfall event can be found in Table 4. For the Seine basin the return period could only be estimated from observations fitted to a Gumbel distribution: 260 years (>60 years). The models indicate a return period of at least 100 years, but probably as high as hundreds of years. In the Loire basin the return period was slightly less extreme, although the best estimate from observations is still 20 years. The lowest estimate from models is 42 years. Note that the model-estimated return periods are not independent of the observations, as the bias correction was based on the same observations as the ones from which the return period was estimated.

Because of the relatively high return period compared to the length of the observed time series, the uncertainties on the return period are quite large. In the near-real-time analysis the return period for the Seine was estimated to be about 180 years (50–3000 years), whereas it is now about 260 years (60–6000 years). For the Loire this was about 35 years (10–300 years), whereas it is now about 20 years (7–170 years). These results are compatible within the large uncertainties.

b. Attribution

The observational records available to us are too short to establish a trend over the last 65 years. We considered five ensembles of climate model experiments to address the question whether the probability of these kinds of events has changed due to anthropogenic emissions of greenhouse gases and aerosols. One relatively coarse-resolution model (EC-Earth 2.3) was not realistic enough for this analysis. To compare the risk ratios from the trend analyses over 1960–2016 with the difference between preindustrial and current conditions, or current conditions without and with anthropogenic forcings, we need to convert the 1960–2016 increase to an

TABLE 5. Summary of the risk ratios found with the different methods, for the two regions and for all used observations and models. Numbers show the best estimate of the GEV fits (Gumbel for observations) and the 95% CIs (in parentheses). The values for HadGEM3-A Nat correspond to a trend in the preindustrial run.

	1960-2016	Preindustrial to 2016
Seine		
E-OBS 14.0	2.1 (0.3–14)	2.4 (0.21–23)
HadGEM3-A	1.9 (1.1–3.4)	2.3 (0.6–7.1)
HadGEM3-A Nat	0.95 (0.5–2.2)	
HadGEM3-A Combined	2.0 (0.7–5.0)	2.3 (0.7–7.1)
weather@home		2.1 (0.6–5.0)
RACMO	2.0 (1.3–4.9)	2.3 (1.4–7.0)
CORDEX	1.6 (0.5–4.9)	1.7 (0.4–7.0)
Loire		
E-OBS 14.0	5.0 (0.7–30)	6.9 (0.4–62)
HadGEM3-A	1.2 (0.8–2.4)	1.2 (0.8–2.9)
HadGEM3-A Nat	1.1 (0.5–1.7)	
HadGEM3-A Combined	1.1 (0.6–3.1)	1.1 (0.5–4.0)
weather@home		1.8 (1.2–2.7)
RACMO	1.8 (1.3–3.2)	2.1 (1.4–4.1)
CORDEX	2.0 (1.1–3.6)	2.4 (1.3–4.8)

estimate of the increase due to anthropogenic forcings. As described in section 2, we do this by applying a scaling factor, assuming that the logarithm of the risk ratio depends linearly on the global mean temperature.

The summary of the risk ratios is given in Table 5. The uncertainty margins on the different model results only include natural variability. The variability between the different models is less than expected on the basis of this natural variability (χ^2/dof < 1), so it is appropriate to use a weighted average with no inflation on the uncertainty range (see section 2). A synthesis of the results for the Seine and the Loire is shown in Fig. 10.

For the Seine, the model spread is well within the range of natural variability (see Fig. 10a). As detailed in section 2, we use a weighted average of the five results and add the uncertainties in quadrature to obtain the combined result. While the single model results and especially the result from observations have large error margins, combining the risk ratios

reduces the error margins and leads to a trend that is significant. The best estimate of the weighted average of the risk ratio between 1880 and 2016 is 2.2, with 95% uncertainty margins ranging from 1.4 to 3.8. This means that we find a significant trend toward more precipitation in the Seine basin for 3-day events similar to or larger than experienced in May/June 2016.

For the Loire, we follow the same procedure as for the synthesis of the RR values of the Seine (see Fig. 10b). The best estimate of the weighted average of the risk ratio between 1880 and 2016 is 1.9, with 95% uncertainty margins ranging from 1.5 to 2.6. This means that, due to the combination of the results, we also find a significant trend to more precipitation in the Loire basin for 3-day events similar to or larger than experienced in May/June 2016.

We can attribute the increase in probability for 3-day averaged precipitation in April–June in the Seine and Loire basins as high as observed in 2016 or higher to anthropogenic climate change using two lines of argument. First, this increase in likelihood is equivalent to an increase in intensity of 6%–7% for a constant return period. This value is in line with the increase in water vapor expected due to the Clausius–Clapeyron relation under a constant relative humidity and a heating of slightly under 1°C of the Mediterranean and subtropical Atlantic Ocean that are potential sources of the moisture here, so the trend in precipitation is related to the trend in SSTs that has been attributed to anthropogenic emissions. More directly, the two analyses that explicitly investigate the difference between natural and natural + anthropogenic forcings give results that are compatible with all the others and together are significantly different from no change, whereas the natural-only runs show no trend. Together this confirms that the trend is to a large extent due to anthropogenic forcings.

The original results in van Oldenborgh et al. (2016) were based on initial precipitation estimates that turned out to be about 10% lower than the area-averaged value that became available later. However, the changes in intensity and probability are not sensitive to such a change in the threshold and the results of this analysis are very similar. In the original results the risk ratio for the Seine basin was estimated to be 2.3 (>1.6), whereas the current analysis gives 2.2 (1.4–3.8). For the Loire basin the original estimate was 2.0 (>1.4), whereas it is now 1.9 (1.5–2.6).
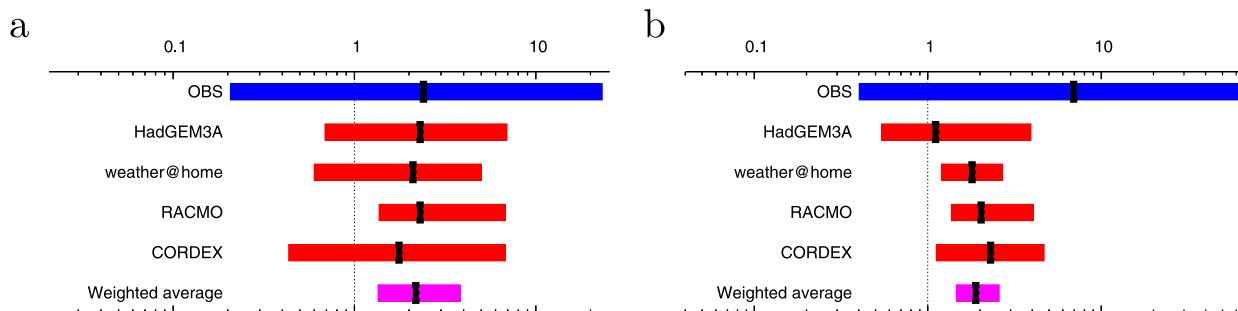

FIG. 10. Synthesis of the risk ratios between 1880 and 2016 for (a) the Seine basin and (b) the Loire basin. Dark blue is for observed precipitation, red is for climate model ensembles. The ranges are compatible with each other and combine to a weighted average (purple).

While this study is not a general proof that all rapid analyses are now "valid" or free of error, it adds to the weight of evidence that rapid analyses can be acceptable and useful. However, in general, as for this case, we expect the trends in intensity or probability of similar events to be relatively insensitive to small changes in the observed event magnitude (threshold).

An unanswered question at the moment is whether a change in the dynamics played a role: have the odds of a stationary cutoff low over this region increased? The methods to answer this question have only been recently developed (Vautard et al. 2016) and have not yet been applied to this event.

REFERENCES

Allen, M. R., and W. J. Ingram, 2002: Constraints on future changes in climate and the hydrologic cycle. *Nature*, **419**, 224–232, https://doi.org/10.1038/nature01092.

Annan, J. D., and J. C. Hargreaves, 2010: Reliability of the CMIP3 ensemble. *Geophys. Res. Lett.*, **37**, L02703, https://doi.org/10.1029/2009GL041994.

Boé, J., and F. Habets, 2014: Multi-decadal river flow variations in France. *Hydrol. Earth Syst. Sci.*, **18**, 691–708, https://doi.org/10.5194/hess-18-691-2014.

Brunelle, J., J. Diribarne, and J. Solignac, 2016: Épisodes de crue de mai-juin 2016 sur le bassin de la Seine. Tech. Rep., 92 pp., http://www.driee.ile-de-france.developpement-durable.gouv.fr/IMG/pdf/rex4m_spc_smyl_mai_juin_2016_vf.pdf.

Christidis, N., P. A. Stott, A. A. Scaife, A. Arribas, G. S. Jones, D. Copsey, J. R. Knight, and W. J. Tennant, 2013: A new HadGEM3-A-based system for attribution of weather- and climate-related extreme events. *J. Climate*, **26**, 2756–2783, https://doi.org/10.1175/JCLI-D-12-00169.1.

Coles, S., 2001: *An Introduction to Statistical Modeling of Extreme Values.* Springer, 208 pp.

Donlon, C. J., M. Martin, J. Stark, J. Roberts-Jones, E. Fiedler, and W. Wimmer, 2012: The Operational Sea Surface Temperature and Sea Ice Analysis (OSTIA) system. *Remote Sens. Environ.*, **116**, 140–158, https://doi.org/10.1016/j.rse.2010.10.017.

Dorchies, D., and Coauthors, 2014: Climate change impacts on multi-objective reservoir management: Case study on the Seine river basin, France. *Int. J. River Basin Manage.*, **12**, 265–283, https://doi.org/10.1080/15715124.2013.865636.

Eden, J. M., K. Wolter, F. E. L. Otto, and G. J. van Oldenborgh, 2016: Multi-method attribution analysis of extreme precipitation in Boulder, Colorado. *Environ. Res. Lett.*, **11**, 124009, https://doi.org/10.1088/1748-9326/11/12/124009.

Efron, B., and R. J. Tibshirani, 1998: *An Introduction to the Bootstrap.* Chapman and Hall, 436 pp.

Faytre, L., 2011: Urbanisation et zones inondables: Les risques encourus. Note Rapide Environnement 557, Institut d'Environnement et d'Urbanisme, 6 pp., https://www.iau-idf.fr/fileadmin/NewEtudes/Etude_848/NR_557_web.pdf.

Ficchì, A., L. Raso, D. Dorchies, F. Pianosi, P.-O. Malaterre, P.-J. van Overloop, and M. Jay-Allemand, 2016: Optimal operation of the multireservoir system in the Seine river basin using deterministic and ensemble forecasts. *J. Water Resour. Plann. Manage.*, **142**, https://doi.org/10.1061/(ASCE)WR.1943-5452.0000571.

Gallet, L., 2016: Ce que l'on sait des quatre victimes des inondations en France. *L'Express*, 4 June, https://www.lexpress.fr/actualite/societe/meteo/que-sait-on-des-quatre-victimes-des-inondations-en-france_1798930.html.

Hagedorn, R., F. J. Doblas-Reyes, and T. N. Palmer, 2005: The rationale behind the success of multi-model ensembles in seasonal forecasting – I. Basic concept. *Tellus*, **57A**, 219–233, https://doi.org/10.1111/j.1600-0870.2005.00103.x.

Hanel, M., T. A. Buishand, and C. A. T. Ferro, 2009: A nonstationary index flood model for precipitation extremes in transient regional climate model simulations. *J. Geophys. Res.*, **114**, D15107, https://doi.org/10.1029/2009JD011712.

Hauser, M., and Coauthors, 2017: Methods and model dependency of extreme event attribution: The 2015 European drought. *Earth's Future*, **5**, 1034–1043, https://doi.org/10.1002/2017EF000612.

Haustein, K., and Coauthors, 2016: Real-time extreme weather event attribution with forecast seasonal SSTs. *Environ. Res. Lett.*, **11**, 064006, https://doi.org/10.1088/1748-9326/11/6/064006.

Hawkins, E., and Coauthors, 2017: Estimating changes in global temperature since the preindustrial period. *Bull. Amer. Meteor. Soc.*, **98**, 1841–1856, https://doi.org/10.1175/BAMS-D-16-0007.1.

Haylock, M. R., N. Hofstra, A. M. G. Klein Tank, E. J. Klok, P. D. Jones, and M. New, 2008: A European daily high-resolution gridded data set of surface temperature and precipitation for 1950–2006. *J. Geophys. Res.*, **113**, D20119, https://doi.org/10.1029/2008JD010201.

Hazeleger, W., and Coauthors, 2010: EC-Earth: A seamless Earth-system prediction approach in action. *Bull. Amer. Meteor. Soc.*, **91**, 1357–1363, https://doi.org/10.1175/2010BAMS2877.1.

Jacob, D., and Coauthors, 2014: EURO-CORDEX: New high-resolution climate change projections for European impact research. *Reg. Environ. Change*, **14**, 563–578, https://doi.org/10.1007/s10113-013-0499-2.

Kirtman, B., and Coauthors, 2013: Near-term climate change: Projections and predictability. *Climate Change 2013: The*

Physical Science Basis, T. F. Stocker et al., Eds., Cambridge University Press, 953–1028.

Lehner, B., K. Verdin, and A. Jarvis, 2008: New global hydrography derived from spaceborne elevation data. *Eos, Trans. Amer. Geophys. Union*, **89**, 93–94, https://doi.org/10.1029/2008EO100001.

Lenderink, G., and E. van Meijgaard, 2008: Increase in hourly precipitation extremes beyond expectations from temperature changes. *Nat. Geosci.*, **1**, 511–514, https://doi.org/10.1038/ngeo262.

Massey, N., and Coauthors, 2015: weather@home—Development and validation of a very large ensemble modelling system for probabilistic event attribution. *Quart. J. Roy. Meteor. Soc.*, **141**, 1528–1545, https://doi.org/10.1002/qj.2455.

Mitchell, D., and Coauthors, 2017: Assessing mid-latitude dynamics in extreme event attribution systems. *Climate Dyn.*, **48**, 3889–3901, https://doi.org/10.1007/s00382-016-3308-z.

Mulholland, R., 2016: France floods 'caused one billion euros worth of damage.' *Telegraph*, 5 June, https://www.telegraph.co.uk/news/2016/06/05/france-floods-caused-one-billion-euros-worth-of-damage/.

Otto, F. E. L., N. Massey, G. J. van Oldenborgh, R. G. Jones, and M. R. Allen, 2012: Reconciling two approaches to attribution of the 2010 Russian heat wave. *Geophys. Res. Lett.*, **39**, L04702, https://doi.org/10.1029/2011GL050422.

——, K. van der Wiel, G. van Oldenborgh, S. Philip, S. Kew, P. Uhe, and H. Cullen, 2018: Climate change increases the probability of heavy rains in northern England/southern Scotland like those of storm Desmond—A real-time event attribution revisited. *Environ. Res. Lett.*, **13**, 024006, https://doi.org/10.1088/1748-9326/aa9663.

Pall, P., T. Aina, D. A. Stone, P. A. Stott, T. Nozawa, A. G. J. Hilberts, D. Lohmann, and M. R. Allen, 2011: Anthropogenic greenhouse gas contribution to flood risk in England and Wales in autumn 2000. *Nature*, **470**, 382–385, https://doi.org/10.1038/nature09762.

Perrin, F., P. Sauzey, B. Menoret, and P.-a. Roche, 2017: Inondations de mai et juin 2016 dans les bassins moyens de la Seine et de la Loire: Retour d'expérience. CGEDD Rep. 010743-01/IGA Rep. 16080-R, 212 pp., http://cgedd.documentation.developpement-durable.gouv.fr/documents/cgedd/010743-01_rapport.pdf .

Prein, A. F., and Coauthors, 2015: A review on regional convection-permitting climate modeling: Demonstrations, prospects, and challenges. *Rev. Geophys.*, **53**, 323–361, https://doi.org/10.1002/2014RG000475.

Quintana-Seguí, P., and Coauthors, 2008: Analysis of near-surface atmospheric variables: Validation of the SAFRAN Analysis over France. *J. Appl. Meteor. Climatol.*, **47**, 92–107, https://doi.org/10.1175/2007JAMC1636.1.

Ribes, A., S. Thao, R. Vautard, B. Dubuisson, S. Somot, J. Colin, S. Planton, and J.-M. Soubeyroux, 2018: Observed increase in extreme daily rainfall in the French Mediterranean. *Climate Dyn.*, https://doi.org/10.1007/s00382-018-4179-2, in press.

Roche, P.-A., 2004: The Seine River flooding in the Ile-de-France region: What account is taken of climate change in the decision-making process? *OECD Global Forum on Sustainable Development: Development and Climate Change*, Paris, OECD, http://www.oecd.org/env/cc/33995401.pdf.

Schaller, N., F. E. L. Otto, G. J. van Oldenborgh, N. R. Massey, S. Sparrow, and M. R. Allen, 2014: The heavy precipitation event of May–June 2013 in the upper Danube and Elbe basins [in "Explaining Extreme Events of 2013 from a Climate Perspective"]. *Bull. Amer. Meteor. Soc.*, **95** (9), S69–S72.

——, and Coauthors, 2016: Human influence on climate in the 2014 southern England winter floods and their impacts. *Nat. Climate Change*, **6**, 627–634, https://doi.org/10.1038/nclimate2927.

Seine Grands Lacs, 2016: Etat et gestion des réservoirs du lundi 06 juin 2016 — situation à 8h. Info lacs en crue no 6, http://seinegrandslacs.fr/sites/default/files/infolacs_crue_20160606.pdf.

Sippel, S., and Coauthors, 2016: A novel bias correction methodology for climate impact simulations. *Earth Syst. Dyn.*, **7**, 71–88, https://doi.org/10.5194/esd-7-71-2016.

Taylor, K. E., R. J. Stouffer, and G. A. Meehl, 2012: An overview of CMIP5 and the experiment design. *Bull. Amer. Meteor. Soc.*, **93**, 485–498, https://doi.org/10.1175/BAMS-D-11-00094.1.

Uhe, P., F. E. L. Otto, K. Haustein, G. J. van Oldenborgh, A. King, D. Wallom, M. R. Allen, and H. Cullen, 2016: Comparison of methods: Attributing the 2014 record European temperatures to human influences. *Geophys. Res. Lett.*, **43**, 8685–8693, https://doi.org/10.1002/2016GL069568.

van den Besselaar, E. J. M., A. M. G. Klein Tank, and T. A. Buishand, 2013: Trends in European precipitation extremes over 1951–2010. *Int. J. Climatol.*, **33**, 2682–2689, https://doi.org/10.1002/joc.3619.

van den Brink, H. W., and G. P. Können, 2008: The statistical distribution of meteorological outliers. *Geophys. Res. Lett.*, **35**, L23702, https://doi.org/10.1029/2008GL035967.

——, and ——, 2011: Estimating 10000-year return values from short time series. *Int. J. Climatol.*, **31**, 115–126, https://doi.org/10.1002/joc.2047.

van der Wiel, K., and Coauthors, 2017: Rapid attribution of the August 2016 flood-inducing extreme precipitation in south Louisiana to climate change. *Hydrol. Earth Syst. Sci.*, **21**, 897–921, https://doi.org/10.5194/hess-21-897-2017.

Van Meijgaard, E., L. H. Van Ulft, W. J. Van de Berg, F. C. Bosveld, B. J. J. M. van den Hurk, G. Lenderink, and A. P. Siebesma, 2008: The KNMI regional atmospheric climate model RACMO version 2.1. Tech. Rep. 302, Koninklijk Nederlands Meteorologisch Instituut, 50 pp., http://bibliotheek.knmi.nl/knmipubTR/TR302.pdf.

——, ——, G. Lenderink, S. R. De Roode, E. L. Wipfler, R. Boers, and R. M. A. van Timmermans, 2012: Refinement and application of a regional atmospheric model for climate scenario calculations of Western Europe. Tech. Rep. KVR 054/12, 44 pp.

van Oldenborgh, G. J., 2007: How unusual was autumn 2006 in Europe? *Climate Past*, **3**, 659–668, https://doi.org/10.5194/cp-3-659-2007.

——, G. Burgers, and A. Klein Tank, 2000: On the El Niño teleconnection to spring precipitation in Europe. *Int. J. Climatol.*, **20**, 565–574, https://doi.org/10.1002/(SICI)1097-0088(200004)20:5<565::AID-JOC488>3.0.CO;2-5.

——, F. J. Doblas Reyes, S. S. Drijfhout, and E. Hawkins, 2013: Reliability of regional climate model trends. *Environ. Res. Lett.*, **8**, 014055, https://doi.org/10.1088/1748-9326/8/1/014055.

——, F. E. L. Otto, K. Haustein, and H. Cullen, 2015: Climate change increases the probability of heavy rains like those of storm Desmond in the UK—An event attribution study in near-real time. *Hydrol. Earth Syst. Sci. Discuss.*, **12**, 13 197–13 216, https://doi.org/10.5194/hessd-12-13197-2015.

——, and Coauthors, 2016: Rapid attribution of the May/June 2016 flood-inducing precipitation in France and Germany to

climate change. *Hydrol. Earth Syst. Sci. Discuss.*, https://doi.org/10.5194/hess-2016-308.

Vautard, R., and Coauthors, 2015: Extreme fall 2014 precipitations in the Cévennes Mountains [in "Explaining Extreme Events of 2014 from a Climate Perspective"]. *Bull. Amer. Meteor. Soc.*, **96** (12), S56–S60, https://doi.org/10.1175/BAMS-D-15-00088.1.

——, P. Yiou, F. E. L. Otto, P. A. Stott, N. Christidis, G. J. van Oldenborgh, and N. Schaller, 2016: Attribution of human-induced dynamical and thermodynamical contributions in extreme weather events. *Environ. Res. Lett.*, **11**, 114009, https://doi.org/10.1088/1748-9326/11/11/114009.

——, and Coauthors, 2018: Evaluation of the HadGEM3-A simulations in view of climate and weather event human influence attribution in Europe. *Climate Dyn.*, https://doi.org/10.1007/s00382-018-4183-6, in press.

Wilson, P. S., and R. Toumi, 2005: A fundamental probability distribution for heavy rainfall. *Geophys. Res. Lett.*, **32**, L14812, https://doi.org/10.1029/2005GL022465.

Yokohata, T., J. Annan, M. Collins, C. Jackson, M. Tobis, M. Webb, and J. Hargreaves, 2012: Reliability of multi-model and structurally different single-model ensembles. *Climate Dyn.*, **39**, 599–616, https://doi.org/10.1007/s00382-011-1203-1.